Int J Thermophys (2012) 33:627–639
DOI 10.1007/s10765-011-1110-z

Thermophysical and Magnetic Properties of Carbon Beads Containing Cobalt Nanocrystallites

M. Izydorzak · A. Skumiel · M. Leonowicz · M. Kaczmarek-Klinowska · A. D. Pomogailo · G. I. Dzhardimalieva

Received: 25 March 2011 / Accepted: 10 October 2011 / Published online: 26 October 2011

Abstract Magnetic Co-beads were fabricated in the course of a three-step procedure comprising preparation of a metal–acrylamide complex, followed by frontal polymerization and finally pyrolysis of the polymer. The composites obtained were composed of cobalt nanocrystallites stabilized in a carbon matrix built of disordered graphite. The crystallite size, material morphology, fraction of the magnetic component, and thus the magnetic properties can be tailored by a proper choice of the processing variables. The samples were subjected to an alternating magnetic field of different strengths ($H = 0$ to $5\ \mathrm{kA \cdot m^{-1}}$) at a frequency of $f = 500$ kHz. From the calorimetric measurements, we concluded that the relaxation processes dominate in the heat generation mechanism for the beads pyrolyzed at 773 K. For the beads pyrolyzed at 1073 K, significant values of magnetic properties, such as the coercive force and remanence give substantial contribution to the energy losses for hysteresis. The specific absorption coefficient (*SAR*) related to the cobalt mass unit for the 1073 K pyrolyzed beads ($SAR = 1340\ \mathrm{W \cdot g_{cobalt}^{-1}}$) is in very good conformity with the results obtained by other authors. The effective density power loss, caused by eddy currents, can be neglected for heating processes applied in magnetic hyperthermia. The Co-beads can potentially be applied for hyperthermia treatment.

M. Izydorzak · M. Leonowicz
Faculty of Materials Science and Engineering, Warsaw University of Technology, Wołoska 141, 02-507 Warsaw, Poland

A. Skumiel (✉) · M. Kaczmarek-Klinowska
Institute of Acoustics, Faculty of Physics, Adam Mickiewicz University, Umultowska 85, 61-614 Poznań, Poland
e-mail: skumiel@amu.edu.pl

A. D. Pomogailo · G. I. Dzhardimalieva
Institute of Chemical Physics RAS, Chernogolovka, Russia

Keywords Carbon nanocomposites · Hyperthermia · Magnetic beads

1 Introduction

Magnetic nanoparticles are leading candidates for medical applications because of their unique multifunctional properties. The same magnetic nanocrystals may serve as a contrast agent for magnetic resonance imaging, as a gene delivery agent, and also as a nanosource of heat. Beyond their potential in medical imaging, nanomagnets can also be used to manipulate labelled entities, as they experience a force when placed in a nonuniform magnetic field [1]. For magnetic hyperthermia, nanoparticles activated by an alternating magnetic field at a frequency of some hundred kHz are usually used. The activation leads to release of heat energy, leading to increasing temperature. This means that the cobalt beads (or other magnetic nanoparticles) can be used in tumor cell therapy. The heat release is based on two physical phenomena: losses for hysteresis and (or) relaxation [2].

In the range of particle diameters above about 100 nm, magnetic multidomain particles react to external magnetic fields by Bloch wall displacement; therefore, a hysteresis loop is a source of energy losses. With decreasing particle size, a transition to single domain particles occurs and energy losses appear as a result of magnetic relaxation [3,4].

When a sample, which contains monodomain magnetic nanoparticles, is placed into an external alternating magnetic field, the magnetic vector M in that sample undergoes reorientation in space following the magnetic field strength vector H. As a result of the phase delay of the magnetic vector M, in relation to the vector H, a part of the magnetic field energy undergoes irreversible conversion into thermal energy. It leads to heating of the magnetic sample, which can be used in biomedicine for therapy that destroys cancerous cells.

If the sample contains only superparamagnetic particles, magnetic relaxation appears and such a sample magnetizes itself according to two mechanisms: by Brown and by Néel relaxation [5].

A characteristic feature of thermal energy losses in AC magnetic field results from a relaxation process and then the volumetric power dissipation is proportional to the square of the magnetic field amplitude, H [5]:

$$P(f, H) = \pi \mu_0 \chi_0 f H^2 \frac{2\pi f \tau}{1 + (2\pi f \tau)^2}, \tag{1}$$

where χ_0 is the equilibrium susceptibility of a magnetic sample, f is the frequency of the alternating magnetic field, τ is the relaxation time, and $\mu_0 = 4\pi \times 10^{-7}\,\mathrm{V \cdot s \cdot A^{-1} \cdot m^{-1}}$ is the permeability of free space.

The imaginary part of the magnetic susceptibility [5] is a function of both the frequency and magnetic field strength H_o according to the following equation:

$$\chi'' = \chi_0 \frac{\omega\tau}{1 + (\omega\tau)^2} = \frac{\mu_0 \phi M_S^2 V}{k_B T} \frac{L(\xi)}{\xi} \frac{\omega\tau}{1 + (\omega\tau)^2}, \tag{2}$$

where $\chi_0 = 3\chi_i\ (\coth\xi - \xi^{-1}) \cdot \xi^{-1}$ is the equilibrium susceptibility of a magnetic fluid, $\chi_i = (\partial M/\partial H)_i$ is the initial susceptibility determined from differentiation of the Langevin relationship, ϕ_V is the volume fraction of particles in the suspension, M_S is the saturation magnetization of the magnetic material, and $\xi = \mu_0 M_S V H/(kT)$ is the parameter of the Langevin function $L(\xi)$.

In this investigation magnetic beads containing cobalt nanocrystallites, were prepared and studied in the light of their potential applications in magnetic heating. From Eq. 2 it follows that for $\omega\tau = 1$, the imaginary part of the magnetic susceptibility χ'', achieves its maximum value. Because of polydispersion, magnetic nanoparticles with small sizes are located in the sample, being the source of relaxation losses, but there are also particles of larger sizes, which are the source of energy losses for hysteresis. From Refs. [6–8] it follows that for particle systems with ferromagnetic behavior (i.e., hysteresis), a power of three is found at low field amplitudes (for Rayleigh losses). Thus, hysteresis losses, for so-called Rayleigh loops, may be well described by a third-order power law. In that case, it can be written as $P \propto H^3$.

2 Measurements

2.1 Procedure

The Co-containing beads were obtained in the course of a three-step procedure. The first step comprised formation of a monomer, by reaction of cobalt II nitrate with an acrylamide. The second step included formation of a polymeric material by frontal polymerization of the monomer. The final step, which produces the nanocomposite, magnetic structure, comprised pyrolysis of the polymer. A more detailed description of the processing route is presented in [9].

2.2 Experimental Methods

For characterization of the structure and microstructure of the Co-containing beads, studies such as: X-ray phase analysis (Rigaku MiniFlexII, $\lambda(\mathrm{Cu\ K}_\alpha) = 0.154\,184$ nm), Raman spectroscopy (Nicolet Almega XR, laser excitation wavelength of 532 nm), transmission electron microscopy (STEM, JEOL JEM 1200 EX), and scanning electron microscopy (SEM, Hitachi S-3500N) were employed. The particle and crystallite size distribution were measured by application of a laser scattering particle size distribution analyzer (Horiba, LA-950) and an image analysis technique, respectively.

The magnetic properties, such as saturation magnetization (M_S), remanence (M_R), and coercive force ($_JH_C$), were recorded at room temperature, in a magnetic field of $\pm 800\ \mathrm{kA \cdot m^{-1}}$, using a vibrating sample magnetometer (VSM, Lake Shore 7410). The percentage content of the metallic component (F_{mc}) was assessed from the comparison of saturation magnetization values obtained for the Co-beads and the bulk cobalt.

The magnetic field frequency $f = 500$ kHz was selected for the sake of the maximum convenient efficiency of the hyperthermal phenomenon. The temperature of the

sample was monitored using a thermocouple (LT Lutron TM-917) [10,11] with an absolute uncertainty of 0.01 °C.

The heating system consisted of a broadband power amplifier, an induction coil (length of 78 mm), and an oscilloscope (Philips). An induction coil formed part of an RLC series circuit (self-inductance $L_o = 15.6\,\mu H$ in air; without a magnetic sample). The magnetic field strength was determined on the basis of a voltage measurement for a dropping resistor ($R = 1\,\Omega$) at voltage resonance (oscilloscope reading). A glass tube containing the sample was thermally isolated by a layer of fabric from the solenoid winding supported on a plastic sleeve. Water (0.1 mL) was added to the vial with magnetic material to provide better thermal contact with the thermocouple.

3 Results and Discussion

3.1 Structure and Microstructure

The pyrolysis temperature (T_p) was initially assessed on a basis of calorimetric studies. Detailed experiments showed that the lowest pyrolysis temperature, which enabled formation of magnetic beads, was 773 K. Thus, the polymeric material was pyrolyzed at two temperatures, 773 K (denoted as CoAAm773) and 1073 K (denoted as CoAAm1073), respectively. The beads were in the form of irregular, micro-sized particles. The shape of the Co-beads did not remarkably change with the pyrolysis temperature. The size of beads can be reduced, which was shown for the sample denoted as CoAAm773. The as-pyrolyzed sample had a bead size distribution ranging from 3 μm to 300 μm. The distribution diagram showed a characteristic bimodal character. The mean bead size, for this material, can be estimated as 48 μm (Fig. 1a, b). The bead size distribution was narrowed by additional milling in a ball mill. After 60 min of milling, the mean bead size was 4 μm, with a size distribution within a narrow range from 1 μm to 9 μm (Fig. 1c, d).

As was revealed using X-ray phase analysis, the volume of the beads contains, in both cases, randomly distributed nanocrystallites of metallic FCC Co (Figs. 2a and 3a). The nanocrystallites obtained at the pyrolysis temperature of 773 K, had a homogeneous size distribution within a range from 7 nm to 18 nm (mean size about 13 nm) (Fig. 2b). Increase of the T_p up to 1073 K resulted in partial deterioration of the nanostructure. Besides the very fine, as small as 6 nm crystallites, some large crystallites, having 50 nm diameter, were observed (Fig. 3b).

The Co-crystallites were embedded in a carbon matrix, consisting of graphite and amorphous carbon. The respective Raman spectra, for these two phases, are shown in Figs. 2c and 3c, where the peak at around $1590\,cm^{-1}$ corresponds to graphite (G line) and the band, at around $1350\,cm^{-1}$ (D line), to amorphous carbon. For the Co-beads obtained at 1073 K, the Raman spectra showed also the presence of cobalt oxides, basically CoO, which apparently forms on the surface of some nanocrystallites, unprotected by a carbon matrix, evidenced by the band in the range from $400\,cm^{-1}$ to $700\,cm^{-1}$.

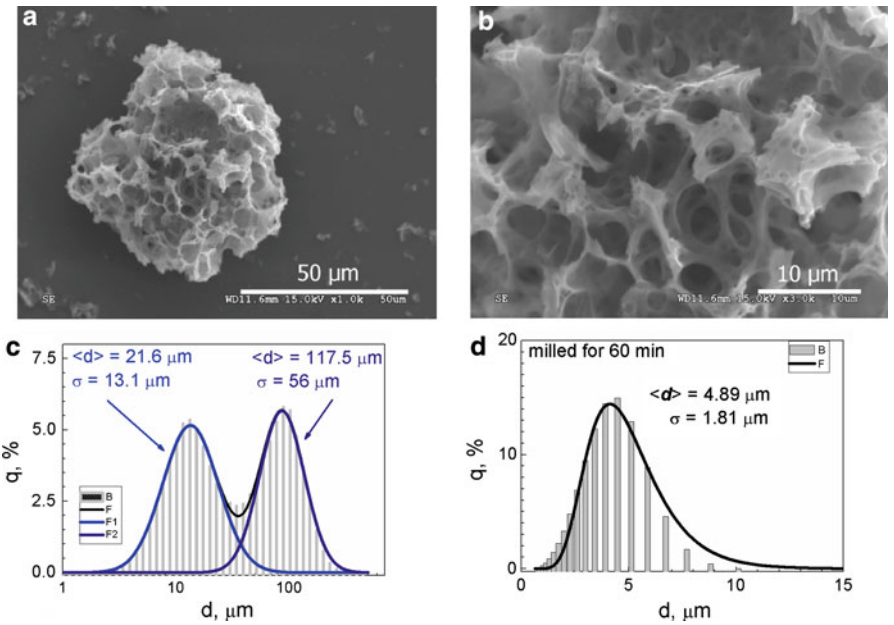

Fig. 1 SEM images of (a, b) CoAAm773, (c) Co-bead size distribution for the as-pyrolyzed sample, and (d) milled for 60 min. *q* represents the quantity of particular fractions

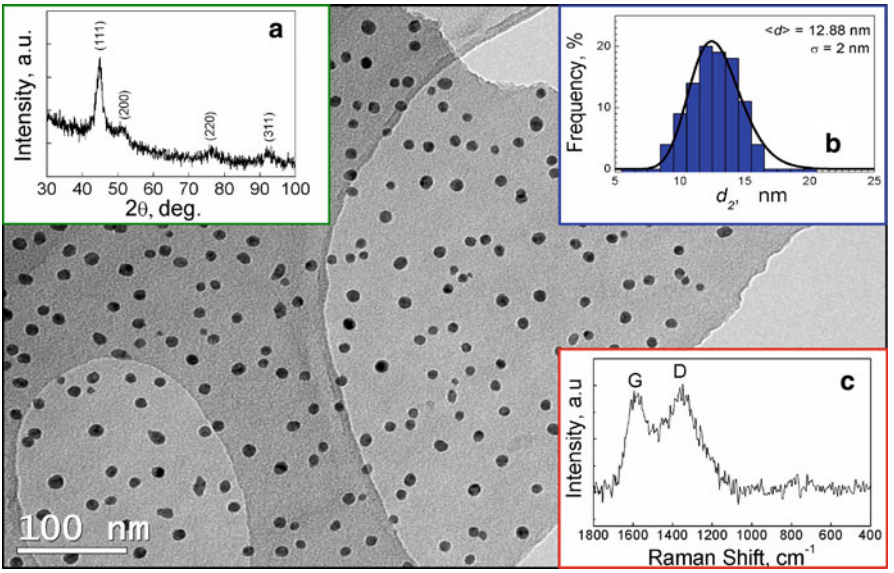

Fig. 2 TEM microtructure of the Co-beads obtained at 773 K: (a) XRD pattern, (b) nanocrystallite size distribution, and (c) Raman spectrum

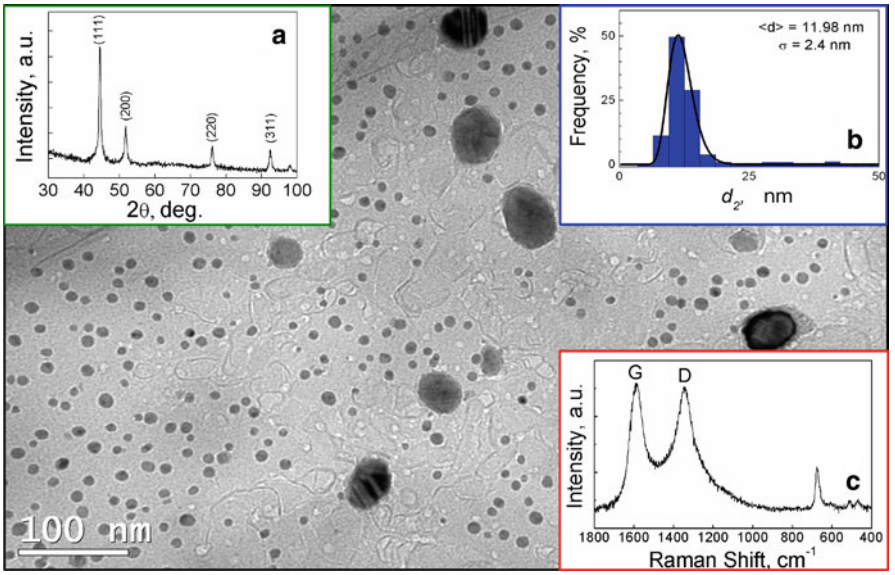

Fig. 3 TEM microtructure of the Co-beads obtained at 1073 K, (a) XRD pattern, (b) nanocrystallite size distribution, and (c) Raman spectrum

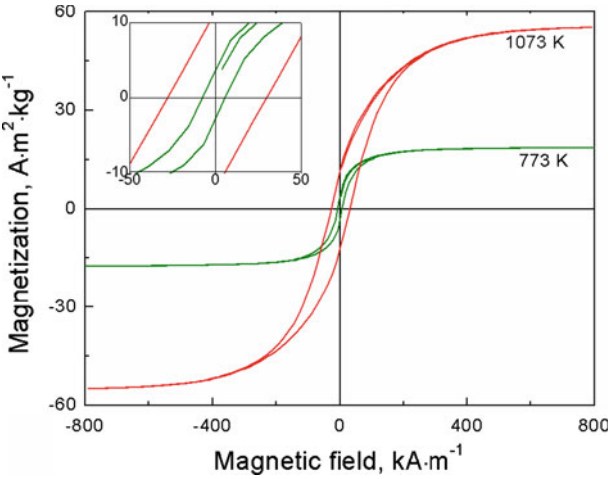

Fig. 4 Room-temperature hysteresis loops for the Co-beads pyrolyzed at 773 K and 1073 K

3.2 Magnetic Properties

The room-temperature magnetic properties of the Co-beads are summarized in Fig. 4 and Table 1. The measurements indicate that, for both pyrolysis temperatures applied, ferromagnetic ordering is dominating. Taking into consideration the presence of ferromagnetic nanocrystallites, the hysteretic component should play an essential

Table 1 Room temperature magnetic properties and fraction of the metallic component for the Co-beads pyrolyzed at 773 K and 1073 K

Sample type	$_{\mathrm{J}}H_{\mathrm{C}}^{\mathrm{a}}$ ($\mathrm{kA \cdot m^{-1}}$)	$M_{\mathrm{R}}^{\mathrm{b}}$ ($\mathrm{A \cdot m^2 \cdot kg^{-1}}$)	$M_{\mathrm{S}}^{\mathrm{c}}$ ($\mathrm{A \cdot m^2 \cdot kg^{-1}}$)	$F_{\mathrm{mc}}^{\mathrm{d}}$ (%)
CoAAm773	6.7	3.6	19.8	12
CoAAm1073	30.5	12.4	55.4	34

[a] Coercive force
[b] Remanence
[c] Saturation magnetization
[d] Fraction of the magnetic component

role in the heat generation mechanism [12,13], especially for the sample denoted as CoAAm1073.

The percentage content of the magnetic component, F_{mc}, was assessed from the simple comparison of the magnetization values for the beads and bulk cobalt ($164\ \mathrm{A \cdot m^2 \cdot kg^{-1}}$ [14]). The F_{mc} values were 12 mass% and 34 mass% for the pyrolysis temperatures of 773 K and 1073 K, respectively. This fact points that elevation of the pyrolysis temperature results not only in a change of the microstructure of the beads but also in an increase of the fraction of the metallic component. This is in correlation with the XRD patterns, which showed that narrower and more intensive peaks were obtained for the Co-beads pyrolyzed at 1073 K, indicating greater amount of the magnetic nanocrystallites, in comparison with the composite produced at 773 K.

The coercive force of the magnetic materials depends on their structure and composition. The pure, elementary metals have usually low coercivity, below $100\ \mathrm{A \cdot m^{-1}}$. A rather high coercive force for the Co-beads, fabricated in this study, can be explained by the partial dissolution of some carbon atoms in the cobalt lattice. The M_{R} values are derivatives of both, the coercive force and saturation magnetization.

3.3 Calorimetric Experiments

A magnetic Co-bead suspension, composed of nanocrystallites stabilized in carbon matrix with added water (to make easy thermal contact with a temperature sensor) was poured into a glass vial. The measurement method was described in detail in [11].

Time-dependent changes of the magnetic sample temperature, for samples subjected to an alternating magnetic field strength H_{AC} at a frequency of $f = 500$ kHz, are presented in Fig. 5. Figure 6a and b presents the rate of temperature increase $(\mathrm{d}T/\mathrm{d}t)_{t=0}$ at the beginning of the heating process as a function of the magnetic field strength H_{AC} in the form of an exponential function. Usually for a sample with both superparamagnetic and ferromagnetic particles, the exponential function [11,15] can be applied,

$$\left(\frac{\mathrm{d}T}{\mathrm{d}t}\right)_{t=0} = \left(\frac{H}{a}\right)^{n}, \tag{3}$$

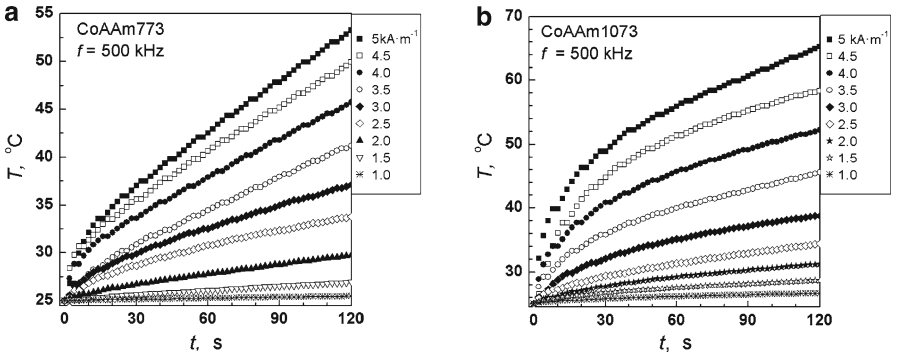

Fig. 5 Time–temperature curves for samples obtained at various pyrolysis temperatures: (a) 773 K and (b) 1073 K, for different values of the magnetic field H_{AC} of frequency $f = 500$ kHz

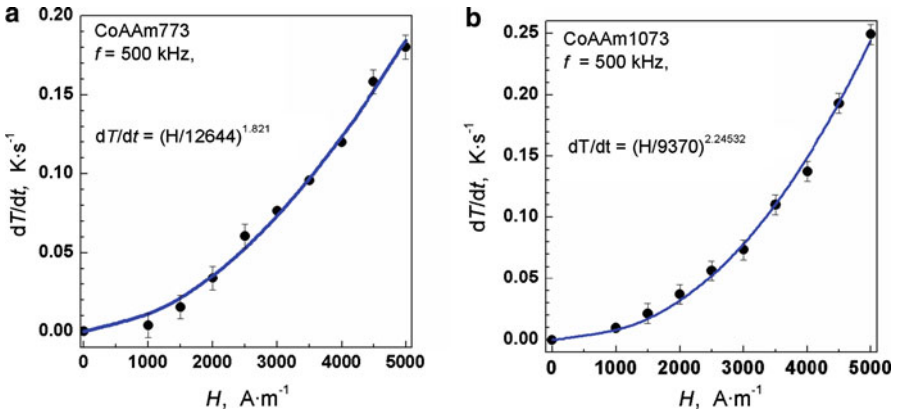

Fig. 6 Dependence of $(\mathrm{d}T/\mathrm{d}t)_{t=0}$ on the alternating magnetic field strength amplitude H at a frequency $f = 500$ kHz for samples pyrolyzed at (a) 773 K and (b) 1073 K

where a and n are the parameters obtained from the fit of the exponential function to the experimental data.

The hyperthermal effect, appearing in the system with superparamagnetic nanoparticles, is characterized by the following square function $(\mathrm{d}T/\mathrm{d}t) \propto H^2$ [3–5,7]. In turn, hysteresis losses, for so-called Rayleigh loops, may well be described by a third-order power law. In that case, it can be written as $P \propto H^3$ [6–8]. However, in practice, the magnetic nanoparticles appear as a polydispersive system and it makes the value $2 \leq n \leq 3$ possible. Hence, when the parameter $n \cong 2$, we can admit that in the tested specimen superparamagnetic nanoparticles dominate, whereas for $n \cong 3$, ferromagnetic particles are in a majority. Astonishingly, for a CoAAm773 sample, the parameter $n = 1.821 \pm 0.079$ points to the existence of only superparamagnetic nanoparticles in the investigated material.

In turn, the parameter $n = 2.245 \pm 0.08$, for the CoAAm1073 sample, indicates the coexistence of both superparamagnetic and ferromagnetic particles. In this case the alternating magnetic field energy is converted into heat by means of relaxation

losses (superparamagnetic particles) accompanying the demagnetization and hysteresis losses (ferromagnetic particles) during the reversal of magnetization [7,8]. Taking into account the principle of energy additivity, we can then write that the released power of losses proportional to $(\mathrm{d}T/\mathrm{d}t)_{t=0}$ consists of two components [8,11]:

$$\left(\frac{\mathrm{d}T}{\mathrm{d}t}\right)_{t=0} = \left(\frac{H}{a}\right)^n = \left(\frac{H}{r}\right)^2 + \left(\frac{H}{h}\right)^3, \tag{4}$$

where r and h are parameters from the fit, which are adequate to describe losses for the relaxational mechanism and hysteresis.

Thus, the last equation for a CoAAm1073 sample can be represented in the following numerical form:

$$\left(\frac{\mathrm{d}T}{\mathrm{d}t}\right)_{t=0} = \left(\frac{H}{9370}\right)^{2.245} = \left(\frac{H}{12159}\right)^2 + \left(\frac{H}{11793}\right)^3. \tag{5}$$

For the CoAAm1073 sample the dependence of $(\mathrm{d}T/\mathrm{d}t)_{t=0}$ on the alternating magnetic field strength H is shown in Fig. 7.

In this figure we can see experimental points (•) and the exponential function $(H/a)^n$ (black line) with its constituents derived from relaxation (blue line) and hysteresis (red line) phenomena. Table 2 presents the values of the parameters obtained from fitting Eq. 4 to the experimental data.

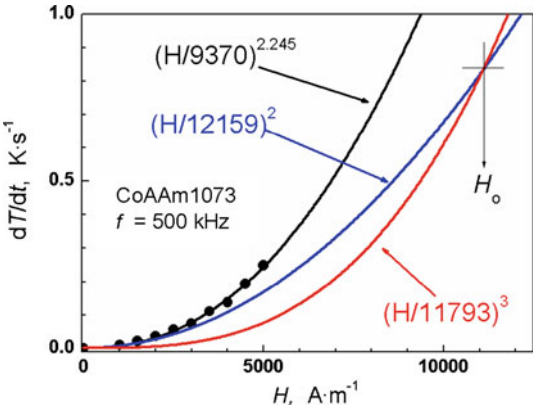

Fig. 7 Dependence of $(\mathrm{d}T/\mathrm{d}t)_{t=0}$ on the alternating magnetic field strength H at frequency $f = 500$ kHz for sample pyrolyzed at 1073 K. Their constituents were derived from relaxation and hysteresis phenomena (Color figure online)

Table 2 Values of the parameters obtained from fitting Eq. 4 to the experimental data

Sample type	a ($\mathrm{A \cdot m^{-1} \cdot s^{1/n} \cdot K^{-1/n}}$)	n (–)	r ($\mathrm{A \cdot m^{-1} \cdot s^{0.5} \cdot K^{-0.5}}$)	h ($\mathrm{A \cdot m^{-1} \cdot s^{1/3} \cdot K^{-1/3}}$)	$H_o = h^3 \cdot r^{-2}$ ($\mathrm{A \cdot m^{-1}}$)
CoAAm773	12644 ± 621	1.821 ± 0.079	12644	–	–
CoAAm1073	9370 ± 274	2.245 ± 0.08	12159 ± 41	11793± 69	11106

From Eq. 5 it follows that the value of the magnetic field strength H_0, at which both components make an equal contribution to the power loss in the sample, amounts to

$$H_0 = \frac{h^3}{r^2}. \tag{6}$$

If $H < H_0$, the relaxation losses dominate, whereas for $H > H_0$, the energy losses, that emerged as a result of a magnetic hysteresis loop, dominate.

The specific absorption rate (*SAR*) defined as the thermal power dissipation divided by the mass of magnetic crystal m_{Co} can be expressed as [1]

$$SAR\left[\frac{\mathrm{W}}{\mathrm{g_{Co}}}\right] = \frac{C_{p\mathrm{S}}\rho_{\mathrm{S}}}{m_{\mathrm{Co}}}\left(\frac{\mathrm{d}T}{\mathrm{d}t}\right)_{t=0}, \tag{7}$$

where all quantities are defined in Table 3. The *SAR* values as a function of magnetic field strength for all tested samples are shown in Fig. 8.

The specific absorption coefficient *SAR* related to the cobalt mass unit can be written in the following numerical form for the CoAAm773 sample,

$$SAR_{773}\left[\frac{\mathrm{W}}{\mathrm{g_{cobalt}}}\right] = 169\left(\frac{H}{12644}\right)^{1.821}, \tag{8a}$$

and for the CoAAm1073 sample,

Table 3 Calorimetric characterizations of studied samples

Quantity	Units	CoAAm773	CoAAm1073
$C_{p\mathrm{S}}$—specific heat capacity of the sample	$\mathrm{J \cdot g^{-1} \cdot K^{-1}}$	1.544	2.096
ρ_{S}—sample density	$\mathrm{g \cdot cm^{-3}}$	2.45	2.4
ρ_{Co}—cobalt density	$\mathrm{g \cdot cm^{-3}}$	8.89	
$C_{p\mathrm{Co}}$—cobalt specific heat capacity	$\mathrm{J \cdot g^{-1} \cdot K^{-1}}$	0.42	
$C_{p\mathrm{H_2O}}$—water specific heat capacity	$\mathrm{J \cdot g^{-1} \cdot K^{-1}}$	4.175	
$C_{p\mathrm{gl}}$—glass specific heat capacity	$\mathrm{J \cdot g^{-1} \cdot K^{-1}}$	0.7	
C_{pp}—powder specific heat capacity	$\mathrm{J \cdot g^{-1} \cdot K^{-1}}$	0.71	
M_{Co}—mass of cobalt grain in a sample	mg	13.44	10.2
m_{Co}—cobalt grain mass per unit volume of the sample	$\mathrm{g \cdot cm^{-3}}$	0.0224	0.034
$m_{\mathrm{H_2O}}$—mass of added water	g	0.358	0.29
m_{gl}—mass of glass in contact with powder	g	1	0.4
m_{p}—mass of powder	g	0.09856	0.0198
SAR (500 kHz, 5 $\mathrm{kA \cdot m^{-1}}$)	$\mathrm{W \cdot g_{cobalt}^{-1}}$	31.2	36.1
SAR (500 kHz, 10 $\mathrm{kA \cdot m^{-1}}$)—by extrapolation	$\mathrm{W \cdot g_{cobalt}^{-1}}$	110	171
SAR (500 kHz, 25 $\mathrm{kA \cdot m^{-1}}$)—by extrapolation	$\mathrm{W \cdot g_{cobalt}^{-1}}$	593	1340

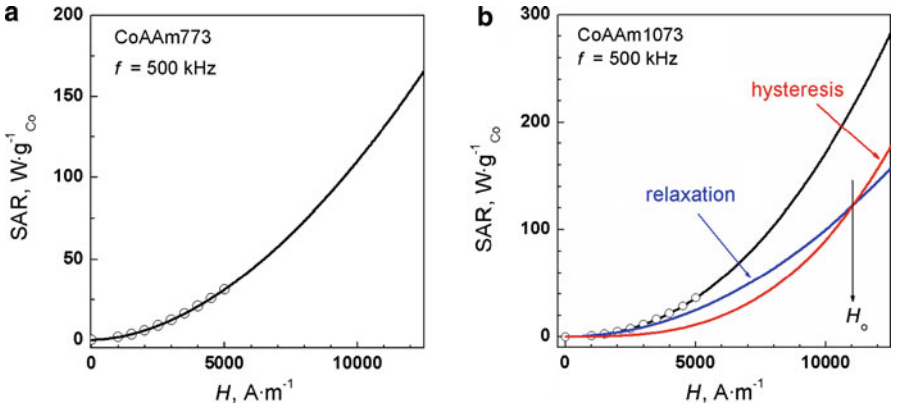

Fig. 8 Specific absorption rate referenced to mass unit of cobalt versus magnetic field strength at a frequency of 500 kHz for both samples at room temperature

$$SAR_{1073}\left[\frac{\mathrm{W}}{\mathrm{g_{cobalt}}}\right] = 148\left(\frac{H}{9370}\right)^{2.245} = 148\left[\left(\frac{H}{12159}\right)^{2} + \left(\frac{H}{11793}\right)^{3}\right]. \tag{8b}$$

For a similar condition described in [12] where $f = 400\,\mathrm{kHz}$ and $H = 25.2\,\mathrm{kA\cdot m^{-1}}$, the authors obtained value of $SAR_{\mathrm{cobalt}} = 1300\,\mathrm{W\cdot g_{cobalt}^{-1}}$. This value is very consistent with our results ($SAR = 1340\,\mathrm{W\cdot g_{cobalt}^{-1}}$) obtained (by extrapolation of Eq. 8b) for the CoAAm1073 sample, which was pyrolyzed at 1073 K. On the other hand, at the field strength of $H = 10\,\mathrm{kA\cdot m^{-1}}$, the quotient SAR_{1073}/SAR_{773} is equal to 1.55. It means that the cobalt beads pyrolyzed at a higher temperature (1073 K) reveal better hyperthermal properties. Therefore, the cobalt beads pyrolyzed at such a temperature can be used in magnetic hyperthermia therapy against tumor cells.

For the sake of a small electrical resistivity ($\rho_{\mathrm{Co}} = 6.25 \times 10^{-8}\,\Omega\cdot\mathrm{m}$) value of cobalt grains, it is worthwhile to try to check the influence of eddy currents on their contribution in total heat losses. Let us consider the single spherical Co-grain (Fig. 9).

A Co-grain placed in an alternating magnetic field of strength $H(t) = H_{\mathrm{o}}\sin(\omega t)$ experiences a magnetic flux for which the value is

$$\varphi(t) = S\mu_{\mathrm{o}}H_{\mathrm{o}}\sin(\omega t), \tag{9}$$

where $S = \pi d^2/4$ is the surface area of the cross section of the magnetic grain, perpendicular to the magnetic vector H. The electric voltage embraced in this way in an external layer of a Co-grain is

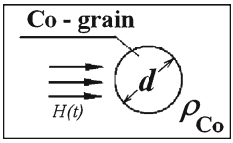

Fig. 9 Electric conducting Co-grain placed in alternating magnetic field

$$U = \frac{\mathrm{d}\varphi(t)}{\mathrm{d}t} = \frac{\pi^2 d^2}{2} f \mu_\mathrm{o} H_\mathrm{o} \cos(\omega t)\,. \tag{10}$$

This voltage around the perimeter of the sphere of diameter d produces in this layer an electrical field strength $E(t)$,

$$E(t) = \frac{\pi d}{2} f \mu_\mathrm{o} H_\mathrm{o} \cos(\omega t)\,. \tag{11}$$

Taking into account the general expression of the temporary density loss power $P(t)$ in the layer with electric resistivity ρ_Co,

$$P(t) = \frac{E^2(t)}{\rho_\mathrm{Co}}, \tag{12}$$

we can obtain its temporary value,

$$P(t) = \frac{E^2(t)}{\rho_\mathrm{Co}} = \frac{(\pi d f \mu_\mathrm{o} H_\mathrm{o})^2}{4\rho_\mathrm{Co}} \cos^2(\omega t)\,. \tag{13}$$

Therefore, the effective density loss power $\langle P \rangle$ equals

$$\langle P \rangle = \frac{E^2_\mathrm{max}(t)}{2\rho_\mathrm{Co}} = \frac{(\pi d f \mu_\mathrm{o} H_\mathrm{o})^2}{8\rho_\mathrm{Co}}. \tag{14}$$

Taking into account the following experimental data: $H_\mathrm{o} = 10\,\mathrm{kA \cdot m^{-1}}$, $f = 5 \times 10^5\,\mathrm{Hz}$, $\mu_\mathrm{o} = 4\pi \times 10^{-7}\,\mathrm{V \cdot s \cdot A^{-1} \cdot m^{-1}}$, and $\rho_\mathrm{Co} = 6.25 \times 10^{-8}\,\Omega \cdot \mathrm{m}$, we obtained the dependence for a Co-grain versus size, which is graphically presented in Fig. 10.

The value of the effective density loss power even for a larger Co-grain (for $d = 50$ nm, $\langle P \rangle = 1.95\,\mathrm{W \cdot m^{-3}}$) received from Eq. 14 can be neglected for a heating

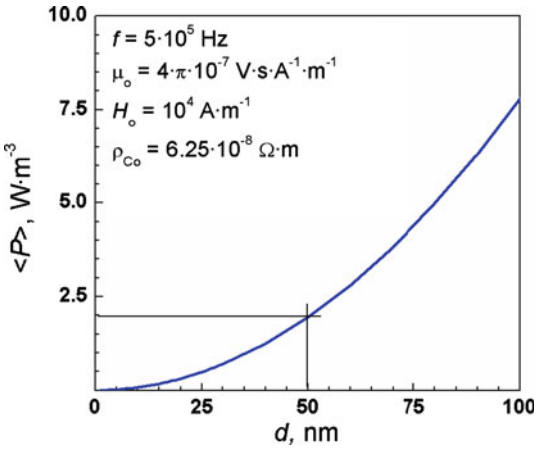

Fig. 10 Effective density loss power $\langle P \rangle$ in electric conducting Co-grain placed in alternating magnetic flux

process which usually is applied in magnetic hyperthermia therapy against tumor cells ($\langle P \rangle \sim 100\,\mathrm{mW \cdot cm^{-3}} = 10^5\,\mathrm{W \cdot m^{-3}}$).

4 Conclusions

On the basis of the experimental work performed in these studies, one can draw the following conclusions:

- The three-step procedure, applied in these studies, enables fabrication of magnetic Co-beads, composed of nanocrystallites stabilized in a carbon matrix.
- It is possible to control the crystallite size, material morphology, fraction of the magnetic component, and thus the magnetic properties by a proper choice of the processing variables.
- From the calorimetric measurements, we conclude that the relaxation processes dominate in the heat generation mechanism for the beads pyrolyzed at 773 K.
- For the beads pyrolyzed at 1073 K, significant values of magnetic properties, such as coercivity and remanence, give substantial contributions to the energy losses for hysteresis.
- The effective density loss power caused by eddy currents can be neglected for the heating process applied in magnetic hyperthermia.

Acknowledgments Financial support from the Ministry of Science and Higher Education (Grant No. N N507 276136) is gratefully acknowledged. The studies were also supported by the Project for Polish-Slovak Bilateral Cooperation No. SK-PL-0069-09/8158/2010.

References

1. J.P. Fortin, C. Wilhelm, J. Servais, C. Ménager, J.C. Bacri, F. Gazeau, J. Am. Chem. Soc. **129**, 2628 (2007)
2. G. Glöckl, R. Hergt, M. Zeisberger, S. Dutz, S. Nagel, W. Weitschies, J. Phys.: Condens. Matter. **18**, 2935 (2006)
3. A.P. Guimaraes, *Principles of Nanomagnetism* (Springer, Heidelberg, 2009)
4. R. Hergt, R. Hiergeist, M. Zeisberger, G. Glöckl, W. Weitschies, L.P. Ramirez, I. Hilger, W.A. Kaiser, J. Magn. Magn. Mater. **280**, 358 (2004)
5. R.E. Rosensweig, J. Magn. Magn. Mater. **252**, 370 (2002)
6. L. Rayleigh, Philos. Mag. **23**, 255 (1887)
7. R. Hergt, W. Andrä, C.G. d'Ambly, I. Hilger, W.A. Kaiser, U. Richter, H.-G. Schmidt, IEEE Trans. Magn. **34**, 3745 (1998)
8. R. Hiergeist, W. Andrä, N. Buske, R. Hergt, I. Hilger, U. Richter, W.A. Kaiser, J. Magn. Magn. Mater. **201**, 420 (1999)
9. A.D. Pomogailo, G.I. Dzhardimaleva, Polym. Sci. Ser. A **3**, 250 (2004)
10. A. Skumiel, J. Magn. Magn. Mater. **307**, 85 (2006)
11. A. Skumiel, Int. J. Thermophys. **31**, 546 (2010)
12. E. Kita, T. Oda, T. Kayano, S. Sato, M. Minagawa, H. Yanagihara, M. Kishimoto, Ch. Mitsumata, S. Hashimoto, K. Yamada, N. Ohkohchi, J. Phys. D: Appl. Phys. **43**, 9 (2010)
13. S.W. Lee, A. Hirukawa, Y.H. Jo, S.G. Lee, IEEE Trans. Nanotechnol. **8**, 86 (2009)
14. R. Pauthenet, J. Appl. Phys. **53**, 8187 (1982)
15. A. Józefczak, A. Skumiel, J. Magn. Magn. Mater. **311**, 193 (2007)